Journal of Materials Chemistry C

Accepted Manuscript

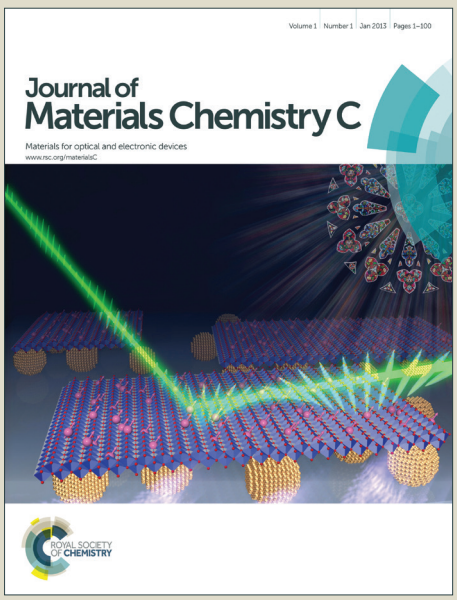

ROYAL SOCIETY OF CHEMISTRY

www.rsc.org/materialsC

Cite this: DOI: 10.1039/c0xx00000x

www.rsc.org/xxxxxx

ARTICLE TYPE

Enhanced red upconversion luminescence by codoping Ce^{3+} in β-$NaY(Gd_{0.4})F_4$: Yb^{3+}/Ho^{3+} nanocrystals

Wei Gao, Hairong Zheng*, Qingyan Han, Enjie He, Fangqi Gao, Ruibo Wang

Received (in XXX, XXX) Xth XXXXXXXXX 20XX, Accepted Xth XXXXXXXXX 20XX

DOI: 10.1039/b000000x

In this work, hexagonal phase $NaY(Gd_{0.4})F_4$: Yb^{3+}/Ho^{3+} nanocrystals were obtained by solvothermal method. The upconversion emission tuning from green to red in $NaY(Gd_{0.4})F_4$: Yb^{3+}/Ho^{3+} nanocrystals was successfully achieved by replacing Y^{3+} ions in the nanocrystal structure with Ce^{3+} ions under 980 nm excitation. The red upconversion emission intensity was enhanced with Ce^{3+} concentration increasing. The output colors for the samples can be clearly observed in a confocal microscopy setup. It was found that two efficient cross-relaxation processes between Ho^{3+} and Ce^{3+} ions had been employed to enhance red emission and suppress green emission. The possible upconversion mechanisms and conversion efficiency between Ho^{3+} and Ce^{3+} ions were investigated in detail. In addition, the influence of the matrix and surface properties on the upconversion emission of the samples were also discussed. The red upconversion emission of Yb^{3+}, Ho^{3+} and Gd^{3+} codoped nanocrystals in this work will have great potential applications in the biological images, magnetic resonance imaging agents, display and anti-counterfeiting applications.

.

1. Introduction

Rare-earth (RE) ion-doped upconversion (UC) materials have presented great potential applications in lighting, solar cell, three-dimensional display, solid-state laser, biological marker and imaging due to their unique emission properties of infrared to visible light.[1-7] Especially, the hexagonal phase $NaYF_4$ crystals have been considered as a most efficient UC emission host materials because of their low phonon energy.[8-10] It was reported that they are bright enough so that single UC nanocrystal with a size of 27 nm on the diameter can be observed in confocal microscopy.[11] Many different synthesis methods have been employed to obtain $NaYF_4$ nonaparticles, including hydrothermal method, solvothermal routes, high-temperature thermal decomposition of trifluoroacetate precursors, and liquid-solid two-phase approaches.[13-16] The structure, morphology and size of nanoparticles are successfully tuned by adjusting the reaction time, temperature, pH value, adding capping agents and codoping different ions.[17-20] For example, Liu and his coworker showed that by introducing additional RE ion, such as Gd^{3+} ion, at a high doping level in $NaYF_4$: Yb^{3+}/Er^{3+} crystallites can decrease the crystallization reaction time and temperature, resulting in ultra-small hexagonal phase UC nanocrystals.[21] In addition, Gd^{3+} doped $NaYF_4$ nanocrystals exhibit paramagnetism at room temperature originating from the intrinsic magnetic moment of Gd^{3+} ions in the host.[22, 23] Hence, Gd^{3+} doped UC nanocrystals have been widely studied as bio-imaging and magnetic resonance imaging agents.

Obtaining a pure single UC emission has been an increasing focus and challenge. The abundance of $4f^N$ electronic states in lanthanide ions typically elicits multicolor fluorescence emission that is tunable from ultraviolet to near-infrared (NIR). Many approaches can produce multicolor UC emissions, which include doping different ions, changing crystal structure, surface modification and tuning particle size and morphology.[24-27] Recently, several attempts have been made to obtain a high-purity, single-band UC red emission that is attractive for anti-counterfeiting and color display applications.[28] High red-to-green emission ratio was achieved by increasing Yb^{3+} concentration in Yb^{3+}/Er^{3+} co-doped $NaYF_4$ nanocrystals.[29] In addition, Mn^{2+} co-doped $NaYF_4$: Yb^{3+}/Er^{3+} nanocrystals exhibited pure single-band red UC emission because of the energy transfer between the Er^{3+} and Mn^{2+} ions.[30] Like Er^{3+}, Ho^{3+} is an intriguing active ion for UC emission because it has a broad fluorescence spectrum that ranges from vacuum ultraviolet to near infrared.[31] Typically, the UC emission from Yb^{3+} and Ho^{3+} codoped systems results in an intense green emission accompanied by a weak red emission.[32-34] However, few reports have been found on the red emission enhancement in Yb^{3+} and Ho^{3+} codoped system. The enhanced red UC emission is observed in LaF_3:Yb^{3+}/Ho^{3+} nanoparticles due to the presence of organic ligands that stabilize the nanoparticles and quench green emission, and high phonon energy host of YVO_4 nanocrystals with high Yb^{3+} concentration.[35, 36] Zhang et

al. had reported that the UC emission from Yb^{3+}/Ho^{3+} co-doped cubic phase $NaYF_4$ nanocrystals was tuned from green to red by introducing Ce^{3+} ions.[37] Trivalent cerium ions have a simple energy structure, and have been considered as an ideal candidate for enhancing the population of intermediate excited state $^5I_7$ of Ho^{3+} that can result in a strong red UC emission.[38] It is well-known that the UC emission intensity of the hexagonal $NaYF_4$ (β-$NaYF_4$) nanocrystals is much stronger than that of the cubic-phase $NaYF_4$ (α-$NaYF_4$) ones.[39-40] Tuning UC fluorescence emission of β-$NaYF_4$:Yb^{3+}/Ho^{3+} nanocrystals from green to red through codoping Ce^{3+} ions will extend their application to color display applications and biological images. However, studies on tuning UC emission in the β-$NaYF_4$:Yb^{3+}/Ho^{3+} nanocrystals through codoping Ce^{3+} ions have been barely reported.[41] In this study, we attempted to tune the UC emission in β-$NaY(Gd_{0.4})F_4$: Yb^{3+}/Ho^{3+} nanorods through codoping with Ce^{3+} ions, and systematically studied their spectral properties with a confocal microscopy setup. The UC emission mechanism and cross-relaxation (CR) processes were investigated carefully.

2. Experimental details

2.1. Materials.

All chemicals used in the current study were analytical graded used without further purification. $Y(NO_3)_3{\cdot}6H_2O$, $Yb(NO_3)_3{\cdot}6H_2O$ $Ho(NO_3)_3{\cdot}6H_2O$ and $Gd(NO_3)_3{\cdot}6H_2O$ are obtained by dissolving Y_2O_3, Yb_2O_3 Ho_2O_3 and Gd_2O_3, (99.99%. Sigma-Aldrich Chemicals Co.) in dilute nitric acid solution at elevated temperature followed by evaporating the superfluous nitric acid, respectively. $Ce(NO_3)_3{\cdot}6H_2O$(99.99%) was purchased from Sigma-Aldrich Chemicals Co.. HNO_3 (65.0%-68.0%), NaF (98.0%), NaOH (98.0%), oleic acid (90.0%) and ethanol (99.7%) were supplied by Sinopharm Chemical Reagent Co, Ltd.

2.2. Synthesis of β-$NaY(Gd_{0.4})F_4$: $Yb^{3+}/Ho^{3+}/Ce^{3+}$ nanocrystals.

β-$NaY(Gd_{0.4})F_4$: $Yb^{3+}/Ho^{3+}/Ce^{3+}$ nanocrystals were synthesized via a solvothermal method by using oleic acid as a stabilizing agent, for which the detailed process is given in reference.[21] 10.0 ml ethanol, 12.0 ml oleic acid and 2.0 ml solution of 0.6 g NaOH were mixed under stirring. Then 1.0 ml of RE $(NO_3)_3$ (0.5 M, RE=Y, Gd, Yb, Ho and Ce) solution and 3.0 ml of NaF (1.0 M) solution were added under vigorous stirring for about 15 minutes. Subsequently, the colloidal solution was transferred into a 40 ml of Telfon-line autoclave and hated at 180℃ for 24 hours. The final products were collected by centrifugation, and washing with deionized water and ethanol for several times. The collected samples were finally dried at 60℃ for several hours.

2.3. Sample characterization and spectral measurement

The powder x-ray diffraction (XRD) were measured with a D/Max2550VB+/PC x-ray diffraction meter with Cu Kα (40 kV, 40 mA) irradiation (λ = 0.15406 nm). The XRD spectra were recorded at a scanning rate of 8° min^{-1}. The morphology of the particles was characterized by the transmission electron microscope (TEM, JEM 2100) and scanning electron microscope (SEM, Quanta 200), respectively. Fourier transform infrared spectroscopy (FTIR) was measured with a Brucher EQUINX55 spectrometer. For spectroscopic measurements, YAG: Nd^{3+} (Quanta Ray Lab-170) pulse laser and Ti sapphire femtosecond laser (Mira-900) were employed as excitation sources. The spectrometer (SP2750i, 0.008 nm) with a PIXIS 100 charge coupled device (CCD, ACTON) and a PD471 photomultiplier tube (PMT, ACTON) was used for luminescence collection and detection. The luminescence photographs were obtained through a confocal microscopy (OLYMPUS-BX51) and camera (Canon 600D). The Proper notch filters were placed in front of the entrance of the monochromator to block the scattering light. All of the spectroscopic measurements are carried out at room temperature.

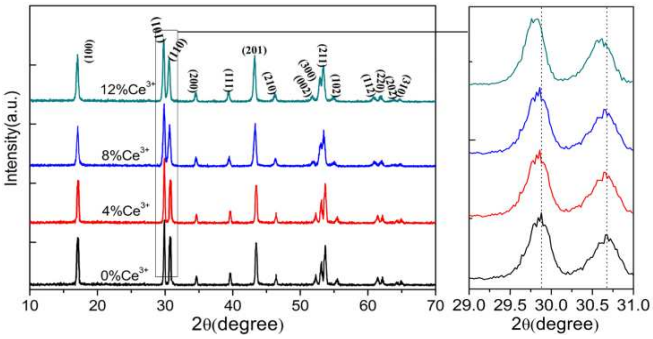

Fig. 1 XRD patterns of $NaY(Gd_{0.4})F_4$: 20%Yb^{3+}/2%Ho^{3+}/xCe^{3+} nanorods (x=0%, 4%, 8% and 12%).

3. Results and discussions

3.1. XRD and TEM

The typical XRD patterns of $NaY(Gd_{0.4})F_4$: 20%Yb^{3+}/2%Ho^{3+} nanocrystals with different Ce^{3+} concentrations are given in Fig. 1. All the strong and sharp diffraction peaks from the samples with or without Ce^{3+} are well indexed to pure hexagonal-phase $NaYF_4$ (JCDPS No. 16-0334). No obvious extra diffraction peaks were detected even with the increase in Ce^{3+} ion concentration to 12%, indicating the formation of a Y-Gd-Ce solid solution. In addition, it is noticed that the diffraction peaks shifted slightly to the low angle side as a result of the increase in unit-cell volume because of the substitution of Y^{3+} (r=0.115 nm) ions by bigger Ce^{3+} (r=0.128 nm) ions in the host lattice (Fig. 1).[42, 43]

Fig. 2 shows typical TME images and EDS spectra of β-$NaY(Gd_{0.4})F_4$: Yb^{3+}/Ho^{3+} nanoparticles with codoping different Ce^{3+} concentrations. A series of Ce^{3+}-doped β-$NaY(Gd_{0.4})F_4$:Yb^{3+}/Ho^{3+} nanorod crystals have an average diameter of 28 nm and a length of 320 nm, as illustrated in Fig. 2(a–c). These results suggested that codoping Ce^{3+} ions had no obvious effect on the size and morphology of the β-$NaY(Gd_{0.4})F_4$: Yb^{3+}/Ho^{3+} nanorods. Further high resolution TEM (HRTEM) image of the nanorod showed an interplanar spacing of 0.52 nm

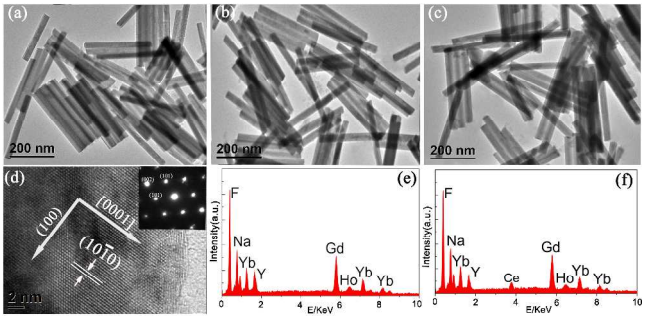

Fig. 2 (a-c) TEM images of β-NaY($Gd_{0.4}$)F_4: 20%Yb^{3+}/2%Ho^{3+} nanorods with Ce^{3+} ions of 0%, 6% and 12%. (d) HRTEM image of β-NaY($Gd_{0.4}$)F_4: 20%Yb^{3+}/2%Ho^{3+} nanorods, and the inset is corresponding the FFT diffraction patterns. (e) and (f) EDS spectrum of β-NaY($Gd_{0.4}$)F_4: 20%Yb^{3+}/2%Ho^{3+}/*x*%Ce^{3+}.

corresponding to the {10$\bar{1}$0} planes of β-NaY($Gd_{0.4}$)F_4 nanorods in Fig. 2(d). This result confirmed that the nanorods grow along the c-axis, namely, the [0001] direction.[44] The fast Fourier transform diffraction patterns obtained from the HRTEM image confirmed that the single crystalline nature of the nanorods, as shown in inset of Fig. 2(d). The incorporation of Ce^{3+} ions was further that the single crystalline nature of the nanorods, as shown in inset of Fig. 2(d). The incorporation of Ce^{3+} ions was further proved by doing the EDS under SEM measurement for β-NaY($Gd_{0.4}$)F_4: 20%Yb^{3+}/2%Ho^{3+} and β-NaY($Gd_{0.4}$)F_4: 20%Yb^{3+}/2%Ho^{3+}/12%Ce^{3+} nanorods, as shown in Fig. 2(e–f). The EDS results confirmed that the main elemental components of the samples are Na, Y, Yb, Ho, Ce, Gd and F in Fig. 2(e–f), the intensity of the Y elemental peak was reduced after introduction of Ce^{3+}, which further indicated that Y^{3+} ions were substituted for Ce^{3+} in β-NaY($Gd_{0.4}$)F_4 host lattice.

3.2. Effective color tuning to the UC emission

3. 2. 1. UC emission and corresponding transitions

The UC luminescence emission of β-NaY($Gd_{0.4}$)F_4:Yb^{3+}/Ho^{3+} nanorods with codoping Ce^{3+} were measured with a confocal microscopy setup. Fig. 3 displays the UC emission spectra, the luminescence photographs, the peak area of the green and red emission, intensity ratio of red to green (R/G) emission, the CIE chromaticity coordinate diagram of β-NaY($Gd_{0.4}$)F_4: Yb^{3+}/Ho^{3+} nanorods with codoping Ce^{3+} concentration from 0% to 12% under NIR 980 nm excitation. The dominant emission peaks at 541 nm and 644 nm are assigned to the transitions of $^5S_2/^5F_4 \rightarrow {}^5I_8$ and $^5F_5 \rightarrow {}^5I_8$ of Ho^{3+} ions in Fig. 3(a).[33, 34] Some weak blue emission (484 nm) and NIR emission (750 nm) can also observed, which are associated with the transition of $^5F_3 \rightarrow {}^5I_8$ and $^5S_2/^5F_4 \rightarrow {}^5I_7$, respectively. Interestingly, with the increase of the Ce^{3+} concentration from 4% to 12%, the increase of green emission is inhibited, and the red emission rise gradually, which can be affirmed by the comparison of peak area of the green and red emission in Fig. 2(b). The output color of β-NaY($Gd_{0.4}$)F_4: Yb^{3+}/Ho^{3+} nanorods is tuned from green to red (in inset of Fig. 3(a)), and the R/G ratio increase from 0.64 to 7.31 in Fig. 3(c). Accordingly the CIE chromaticity coordinate (*x, y*) is also changed from (0.2811, 0.6624) to (0.6110, 0.3106) as the Ce^{3+} concentration increase from 0% to 12% in Table 1, which is an

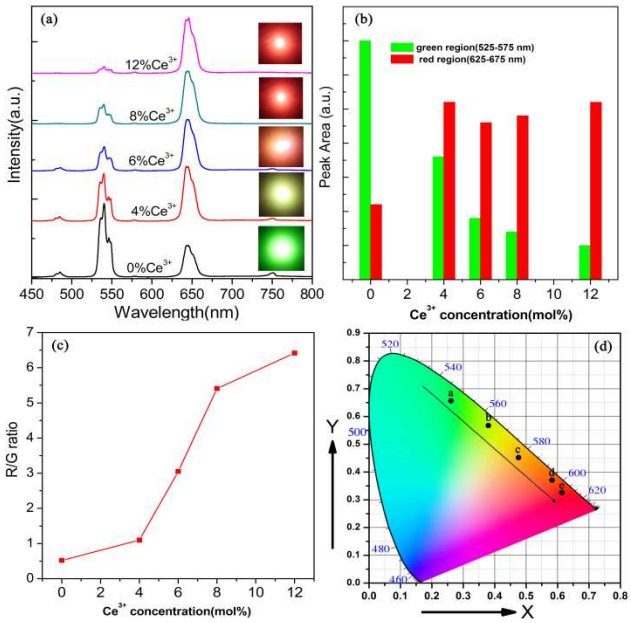

Fig. 3 UC emission spectra (a), the peak area of the green and red emission (b), R/G ratio (c) and CIE chromaticity diagram (d) of β-NaY($Gd_{0.4}$)F_4: Yb^{3+}/Ho^{3+}/Ce^{3+} as a function of Ce^{3+} ion concentration. The inset is corresponding luminescence photograph.

Table 1 The calculated CIE chromaticity coordinate (*x, y*) of β-NaY($Gd_{0.4}$)F_4: 20%Yb^{3+}/2%Ho^{3+} nanorods with different Ce^{3+} concentration.

		CIE chromaticity coordinate	
Point	Samples	*X*	*Y*
a	β-NaY($Gd_{0.4}$)F_4: 20%Yb^{3+}/2%Ho^{3+}	0.2811	0.6624
b	β-NaY($Gd_{0.4}$)F_4: 20%Yb^{3+}/2%Ho^{3+}/ 4%Ce^{3+}	0.3805	0.5741
c	β-NaY($Gd_{0.4}$)F_4: 20%Yb^{3+}/2%Ho^{3+}/ 6%Ce^{3+}	0.4728	0.4504
d	β-NaY($Gd_{0.4}$)F_4: 20%Yb^{3+}/2%Ho^{3+}/ 8%Ce^{3+}	0.5832	0.3734
e	β-NaY($Gd_{0.4}$)F_4: 20%Yb^{3+}/2%Ho^{3+}/ 12%Ce^{3+}	0.6110	0.3106

obvious indication of the luminescence color change. The region of tunable luminescence color in β-NaY($Gd_{0.4}$)F_4:Yb^{3+}/Ho^{3+} nanorods with different Ce^{3+} concentration is shown in Fig. 3(d).

To understand the observed phenomenon, the energy levels and possible relaxations and transitions of Yb^{3+}/Ho^{3+}/Ce^{3+} system were illustrated in Fig. 4. It is know that Yb^{3+} ions have a larger absorption cross-section for infrared light and longer excited state lifetime than that of Ho^{3+}. Thus, the main pathway is assumed to populate the upper emitting states of Ho^{3+} ions should be through the energy transfer from Yb^{3+} to Ho^{3+} ions. Under NIR 980 nm excitation, $^5I_6$, $^5F_5$, and $^5S_2/^5F_4$ states of Ho^{3+} were populated through three successive energy transfer (ET) processes from Yb^{3+} to Ho^{3+}. The strong green (541 nm) and very weak NIR (750 nm) emissions can be generated through radiative relaxations from the $^5F_4/^5S_2$ states to the $^5I_8$ and $^5I_7$ states. The transition from $^5F_5$ state to $^5I_8$ ground state produces strong red UC emission at 644 nm. There are two possible processes to populate the excited state $^5F_5$. One is the nonradiative transition from higher excited states of $^5F_4/^5S_2$.The other is the populationof the long-lived $^5I_7$ level initially by the nonradiative $^5I_6 \rightarrow {}^5I_7$ or by radiative decay of $^5F_4/^5S_2 \rightarrow {}^5I_7$, then, populating the $^5F_5$ level of $^5F_4/^5S_2 \rightarrow {}^5I_7$, then, populating the $^5F_5$ level through the ET process from Yb^{3+} to Ho^{3+}. However, the nonradiative transition

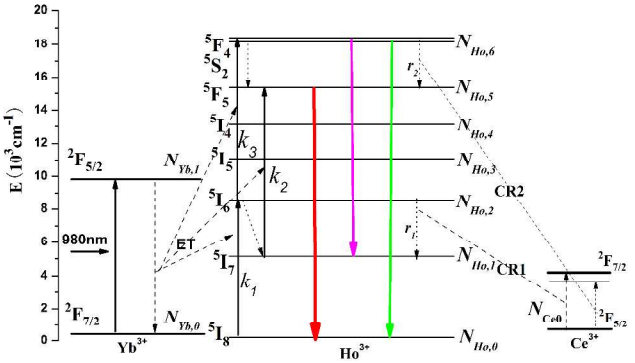

Fig. 4 Energy level diagrams of Ho^{3+}, Yb^{3+} and Ce^{3+} ions as well as proposed UC mechanisms.

probability strongly depends on the phonon energy of the host lattice. The multiphonon nonradiative relaxation rate $W_{NR}(T)$ can be expressed by [45]

$$W_{NR}(T) = W(0)\left[1-\exp\left(\frac{-h\nu}{kT}\right)\right]^{\frac{\Delta E}{h\nu}} \quad (1)$$

where $W_{NR}(T)$ is the rate at temperature T; ΔE is the energy gap between two energy levels; and $h\nu$ is the phonon energy of the host. According to the energy gap law, nonradiative transitions can barely occur when the gap between the two energy states in an activator is much larger than that of the vibration energy of the host lattice.[44] Thus, the mentioned two nonradiative relaxation processes should not efficient because both energy gaps are about 3000 cm^{-1} large which is approximately eight times that of the maximum phonon energy of $NaYF_4$ host (370 cm^{-1}).[8, 47] This explains the experimental observation of relatively weaker red emission and small R/G ratio in the UC luminescence spectra for the samples before Ce^{3+} ions are codoped (see Fig. 3).

3. 2. 2. Effective color tuning by Ce^{3+} ions

As it is presented in the Fig. 3, the red emission is increased when Ce^{3+} is introduced into the system, and the overall color of the UC emission is gradually tuned to red. In order to investigate the mechanism of tunable color induced by different amount Ce^{3+}, the pumping power dependence of the green and red emission of β-$NaY(Gd_{0.4})F_4$: 20%Yb^{3+}/2%Ho^{3+} nanorods with codoping Ce^{3+} was firstly measured, as shown in Fig. 5. The slopes of 1.91 and 1.86 of the green and red emission of β-$NaY(Gd_{0.4})F_4$: 20%Yb^{3+}/2%Ho^{3+} nanorods were yielded by fitting the experimental data in Fig. 5(a), and the slopes of 1.81 and 1.71 of the green and red emission of β-$NaY(Gd_{0.4})F_4$: 20%Yb^{3+}/2%Ho^{3+}/12%Ce^{3+} were yielded by fitting the experimental data in Fig. 5(b). It is should note that the slopes of red emission in β-$NaY(Gd_{0.4})F_4$: 20%Yb^{3+}/2%Ho^{3+}/12%Ce^{3+} nanorods were slightly smaller than that without codoping Ce^{3+} in β-$NaY(Gd_{0.4})F_4$: 20%Yb^{3+}/2%Ho^{3+} nanorods. This was mainly attributed to the two-photon $^5S_2/^5F_4 \rightarrow {}^5I_7$ process, populating the intermediate level of the UC red in β-$NaY(Gd_{0.4})F_4$: 20%Yb^{3+}/2%Ho^{3+} nanorods is canceled in β-$NaY(Gd_{0.4})F_4$: 20%Yb^{3+}/2%Ho^{3+}/12%Ce^{3+} nanorods due to the quenching of the green UC emission. To explore the mechanism of Ce^{3+} to change the emission of Ho^{3+}, we plot the energy diagram of Ce^{3+} to the right side of Ho^{3+} in the Fig. 4. Considering that the energy gap

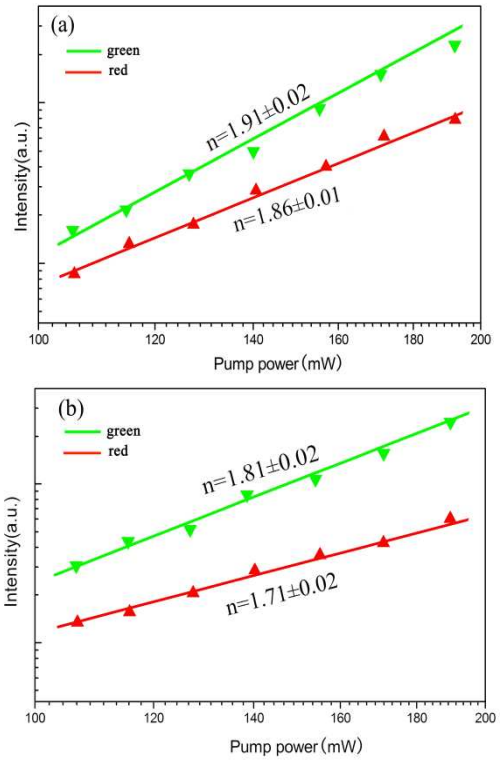

Fig. 5 Pump power dependences of β-$NaY(Gd_{0.4})F_4$: 20%Yb^{3+}/2%Ho^{3+}/x%Ce^{3+} nanorods (x=0% (a) and 12% (b)).

of Ce^{3+} is also about 3000 cm^{-1}, which is similar to the non-radiation relaxation gaps of Ho^{3+} that are involved in the red emissions, the possible cross relaxation process between Ce^{3+} and Ho^{3+} could effectively increase the population of the $^5F_5$ and $^5I_7$ of Ho^{3+}, leading to the enhancement of red emission. Specifically, the CR processes of $^5S_2/^5F_4$ (Ho^{3+}) + $^2F_{5/2}$ (Ce^{3+}) →$^5F_5$ (Ho^{3+}) + $^2F_{7/2}$ (Ce^{3+}) and $^5I_6$ (Ho^{3+}) + $^2F_{5/2}$ (Ce^{3+}) →$^5I_7$ (Ho^{3+}) + $^2F_{7/2}$ (Ce^{3+}) occurred after Ce^{3+} is codoped to the β-$NaY(Gd_{0.4})F_4$: Yb^{3+}/Ho^{3+} system. These two resonant energy transfer processes can effectively increase the populations of $^5F_5$ and $^5I_7$ states from the $^5S_2/^5F_4$ and $^5I_6$ states, thereby increasing the red emission and reducing the green emission.

The steady-state rate equations were established based on the UC processes in Yb^{3+} and Ho^{3+} ion systems in order to further verify the proposed UC mechanism and explain an enhancement of the red emission due to the presence of Ce^{3+} codoping. We firstly introduce $N_{Ho(Yb),i}$, W_i, and W_{ij} (i>j, i, j=0, 1, 2, 3, 4, 5 and 6) to denote the population densities, radiative, and nonradiative transition rates of $^5I_8$, $^5I_7$, $^5I_6$, $^5I_5$, $^5I_4$, $^5F_5$ and $^5S_2/^5F_4$ states of Ho^{3+}, and $^2F_{7/2}$ and $^2F_{5/2}$ of Yb^{3+} ions, respectively. k_1, k_2 and k_3 are defined as energy transfer rates from the excited Yb^{3+} to $^5I_6$, $^5F_5$, and $^5S_2/^5F_4$ states of Ho^{3+} ions, respectively. r_1 and r_2 are the cross-relaxations coefficients between Ho^{3+} and Ce^{3+} at $^5I_6$ and $^5S_2/^5F_4$ states, the N_{Ce0} denotes the population density of the ground state $^2F_{5/2}$ of Ce^{3+} ions. Considering that the radiative relaxation probability of the $^5I_5$ and $^5I_4$ states is very low due to the small neighbored energy gap, we thus ignore the terms of radiation rates in the rate equations. Thus, the rate equations for the discussed system are formulated as follows:[37]

$$\frac{dN_{Ho,1}}{dt} = W_{21}N_{Ho,2} + r_1N_{Ho,2}N_{Ce0} - W_1N_{Ho,1} - k_2N_{Yb,1}N_{Ho,1} \quad (2a)$$

$$\frac{dN_{Ho,2}}{dt} = k_1N_{Yb,1}N_{Ho,0} - W_{21}N_{Ho,2} - r_1N_{Ho,2}N_{Ce0} - W_2N_{Ho,2} - k_3N_{Yb,1}N_{Ho,2} \quad (2b)$$

$$\frac{dN_{Ho,5}}{dt} = k_2N_{Yb,1}N_{Ho,1} + r_2N_{Ho,6}N_{Ce0} - W_5N_{Ho,5} \quad (2c)$$

$$\frac{dN_{Ho,6}}{dt} = k_3N_{Yb,1}N_{Ho,2} - W_6N_{Ho,6} - r_2N_{Ho,6}N_{Ce0} \quad (2d)$$

Taking dN_i/dt=0, and solving the equations 2(a) to 2(d), one can get the following formula for $N_{Ho,2}$, $N_{Ho,5}$ and $N_{Ho,6}$.

$$N_{Ho,2} = \frac{N_{Ho,0}k_1}{(W_{21} + W_2 + r_1N_{Ce0} + k_3N_{Yb,1})}N_{Yb,1} \quad (3)$$

$$N_{Ho,5} = \frac{\left[(W_{21} + r_1N_{Ce0})k_2W_6 + N_{Ce0}r_2(W_1k_3 + r_1N_{Ce0}k_1 + k_2W_{21} + k_2k_3N_{Yb,1})\right]}{W_5(W_6 + N_{Ce0}r_2)(W_1 + k_2N_{Yb,1})(W_{21} + W_2 + r_1N_{Ce0} + k_3N_{Yb,1})}k_1N_{Ho,0}N_{Yb,1}^2 \quad (4)$$

$$N_{Ho,6} = \frac{k_3k_1N_{Ho,0}N_{Yb,1}^2}{(W_6 + r_2N_{Ce0})(W_{21} + W_2 + r_1N_{Ce0} + k_3N_{Yb,1})} \quad (5)$$

Based on equations (4) and (5), we can get the mathematical expression of R/G ratio:

$$\frac{I_{red}}{I_{green}} = \frac{W_5N_{Ho,5}v_{red}}{W_6N_{Ho,6}v_{green}} = \frac{(W_{21} + r_1N_{Ce0})k_2W_6 + N_{Ce0}r_2(W_1k_3 + r_1N_{Ce0}k_1 + k_2W_{21} + k_2k_3N_{Yb,1}))k_1N_{Ho,0}v_{red}}{W_6(W_1 + k_2N_{Yb,1})k_3v_{green}} \quad (6)$$

Thus, the R/G ratio increases with the increase of r_1 and r_2. However, the r_1 and r_2 are decided by the distance of doping ions. The distance between the ions affect the energy transfer between them, therefore, with increase of Ce^{3+} concentration, the value of r_1 and r_2 should increase, leading to the enhancement of red emission from Ho^{3+}. This agrees well with experimental observation (see Fig. 3(a)).

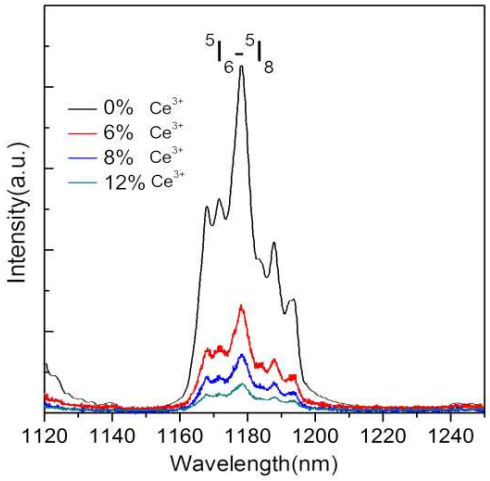

Fig. 6 The NIR ($^5I_6 \rightarrow {}^5I_8$) emission spectra of β-$NaY(Gd_{0.4})F_4$: 20%$Yb^{3+}$/2%$Ho^{3+}$ nanorods as a function of Ce^{3+} ions concentration under 980 nm excitation.

The effect of Ce^{3+} concentration on the enhancement of transitions between Ho^{3+} and Ce^{3+} can be further proved by observing NIR emission of Ho^{3+} at 1180 nm. Fig. 6 shows the NIR emission of $^5I_6 \rightarrow {}^5I_8$ transition of Ho^{3+} ions in β-$NaY(Gd_{0.4})F_4$: 20%Yb^{3+}/2%Ho^{3+} nanorods with codoping Ce^{3+} concentration from 0% to 12% under 980 nm. The NIR emission intensity decreases with Ce^{3+} concentration increasing, which demonstrates the occurrence of CR1 of $^5I_6$ (Ho^{3+}) + $^2F_{5/2}$ (Ce^{3+}) $\rightarrow {}^5I_7$ (Ho^{3+}) + $^2F_{7/2}$ (Ce^{3+}). The radiative transition rates of the $^5I_6$ and $^5I_7$ states of Ho^{3+} ions are supposed to be much larger than their UC emission rates.[37] Thus, the UC emission rates can be ignored in the equations (3). According to equation (3), we can get

$$I_{NIR} = N_{Ho,2}h\nu_{NIR}W_2 = \frac{W_2}{W_2 + r_1N_{Ce0}}h\nu_{NIR}k_1N_{Ho,0}N_{Yb,1} \quad (7)$$

Base on the equation (7) and the measured relative fluorescent intensity in Fig. 6, we get

$$\frac{I_{NIR}(0\%Ce)}{I_{NIR}(12\%Ce)} = \frac{W_2 + r_1N_{Ce0}}{W_2} = 1 + \frac{r_1N_{Ce0}}{W_2} = 0.52 \quad (8)$$

The conversion efficiency of the CR1 process is

$$\eta_1 = \frac{W_{21} + r_1N_{Ce0}}{W_2 + r_1N_{Ce0}} \approx \frac{r_1N_{Ce0}}{W_2 + r_1N_{Ce0}} = \frac{1}{1 + \frac{W_2}{r_1N_{Ce0}}} = 80.6\% \quad (9)$$

This result indicates that the CR1 process of $^5I_6$ (Ho^{3+}) + $^2F_{5/2}$ (Ce^{3+}) $\rightarrow {}^5I_7$ (Ho^{3+}) + $^2F_{7/2}$ (Ce^{3+}) is very efficient.

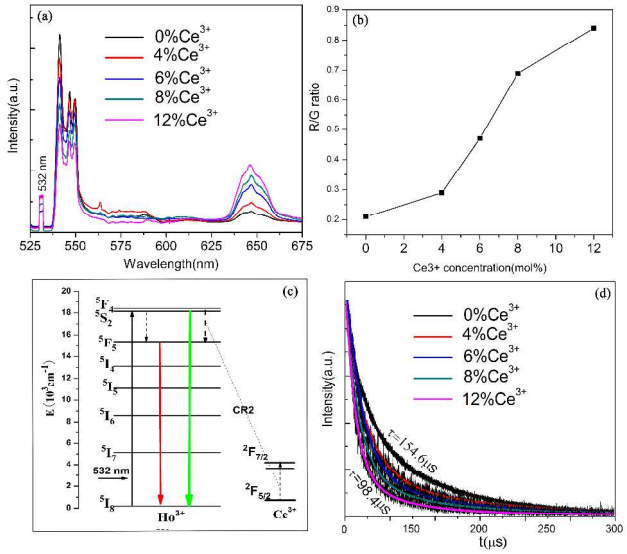

Fig. 7 The down-conversion emission spectra (a), R/G ratio (b) and intensity decay of the green emission ($^5S_2/^5F_4 \rightarrow {}^5I_8$) at 541 nm (d) of β-$NaY(Gd_{0.4})F_4$: 20%$Yb^{3+}$/2%$Ho^{3+}$ nanorods with different Ce^{3+} ions concentration under pulse laser 532 nm excitation. (c) The energy level diagrams of Ho^{3+} and Ce^{3+} ions as well as proposed emission mechanisms.

To test the occurrence of CR2 process of $^5S_2/^5F_4$ (Ho^{3+}) + $^2F_{5/2}$ (Ce^{3+}) $\rightarrow {}^5F_5$ (Ho^{3+}) + $^2F_{7/2}$ (Ce^{3+}) between Ho^{3+} and Ce^{3+} ions. We took the 532 nm photons directly excited Ho^{3+} into the $^5S_2(^5F_4)$ excited states. The down-conversion emission spectra of β-$NaY(Gd_{0.4})F_4$: 20%Yb^{3+}/2%Ho^{3+} nanorods with different Ce^{3+} concentration is shown in Fig. 7(a). It was found that the green

UC emission intensity was reduced, while the red UC emission was increased with increasing Ce^{3+} concentration, and the corresponding R/G ratio was changed from 0.22 to 0.85 in Fig.7(b). According to the energy level diagram of Ho^{3+}, the population of $^5F_5$ state mostly originated from $^5S_2/^5F_4$ excited states through the nonradiative relaxation in Fig. 7(c). Thus, the enhancement of red emission can effectively indicate the occurrence of CR2 process of $^5S_2/^5F_4$ (Ho^{3+}) + $^2F_{5/2}$ (Ce^{3+}) $\rightarrow$$^5F_5$ (Ho^{3+}) + $^2F_{7/2}$ (Ce^{3+}) between Ho^{3+} and Ce^{3+}. The conversion efficiency of the CR2 process can be calculated based on the following equation:[48]

$$\eta_2 = 1 - \frac{\tau(12\%Ce)}{\tau'(0\%Ce)} \quad (10)$$

where τ and τ′ are the decay time of Ho^{3+} with and without the presence of Ce^{3+} in the sample, respectively. The measured fluorescence decay times of $^5S_2/^5F_4$ state are 154.6 μs and 98.4 μs for 0% and 12% Ce^{3+} (Fig. 7(b)), respectively. Thus, the efficiency η_2 is 36.3% for 12% Ce^{3+} ions doped sample. This result indicates that the CR2 process plays the assistant role for the CR1 process to covert the green UC emission into red UC emission.

4. 2. 3. The possible influence of the surface and matrix properties

It is well know that the UC efficiency of nanocrystals depends on the surface impurity and the matrix properties, which mean that the presence of organic ligands on the surface of the samples could also result in the enhancement of red emission. Hence, it is necessary to measure FTIR spectrum for identifying the chemical bonds at the sample surface. Fig. 8 presents the FTIR spectrum with different Ce^{3+} concentration. Several vibration bands were observed from β-$NaY(Gd_{0.4})F_4$: Yb^{3+}/Ho^{3+} nanorods with different Ce^{3+} concentration. The bands in the regions 1350 cm^{-1} to 1700 cm^{-1} and 2800 cm^{-1} to 3050 cm^{-1} corresponded to the vibrations of the C=O and CH_2 groups in the oleic acid, respectively; whereas the broad band at around 3450 cm^{-1} is ascribed to the O–H stretching vibration that originated from the oleic acid and water.[49] These results show the existence of capping ligands on the surface of samples, but no evident change is detected after Ce^{3+} is introduced to the samples, even when its concentration is increased to 12%. This indicates that the possible nonradiative relaxations from the surface capping ligands of the nanorods are not rampant even when Ce^{3+} ion is codoped in the host, which suggests that the output color tuning of the UC emission is caused by the CR processes between Ho^{3+} and Ce^{3+}. More samples including the β-$NaYF_4$: Yb^{3+}/Ho^{3+} microplates and microprisms codoping with Ce^{3+} ions were also prepared for studying the morphology and matrix dependence of the discussed color tuning with Ce^{3+} ions. The XRD, SEM, EDS and CIE chromaticity (*x, y*) of the β-$NaYF_4$: Yb^{3+}/Ho^{3+} microplates and microprisms with codoping Ce^{3+} concentration of 0%, 4%, 6%, 8% and 12% are shown in Fig. S1†, S2† and Table S1†. The stronger diffraction peaks of XRD patterns (Fig. S1†) of β-$NaYF_4$: Yb^{3+}/Ho^{3+} microplates and microprisms with codoping Ce^{3+} ions indicates that they have high crystallinity. Fig. S2† shows that β-

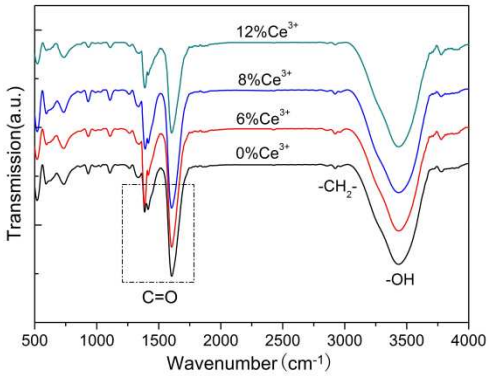

Fig. 8 FTIR spectra of the β-$NaY(Gd_{0.4})F_4$:20%Yb^{3+}/2%Ho^{3+} nanorods with different Ce^{3+} concentration from 0% to 12%.

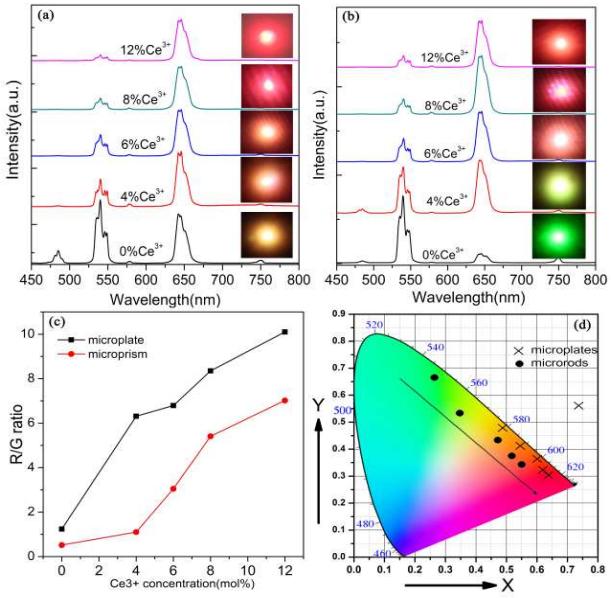

Fig. 9 UC emission spectra and luminescence photographs of β-$NaYF_4$:20%Yb^{3+}/2%Ho^{3+}/*x*Ce^{3+} microplates (a) and microprisms (b) with *x*=0%, 4%, 6%, 8%, 12%. (c) and (d) are the R/G ratio and CIE chromaticity diagrams as a function of Ce^{3+} concentration.

$NaYF_4$ particles are regular microplates and microprisms, and codoping of Ce^{3+} have no effect on the morphology of β- $NaYF_4$ crystals. The spectral measurement on the UC emissions from Ho^{3+} in two groups of β-$NaYF_4$: Yb^{3+}/Ho^{3+} crystals with different shapes present similar color change by a third codopant Ce^{3+}, which is presented in Fig. 9(a-b). The R/G ratio of the microplates and microprisms are increased from 1.24 to 10.06 and from 0.52 to 7.02, respectively, as shown in Fig. 9(c). The corresponding luminescence photographs are shown by the inset of Fig. 9(a) and (b). The CIE chromaticity coordinates for microplates and microprisms are approaching to red region from yellow and green region, respectively, as shown in Fig. 9(d). Thus, the UC emission of β-$NaYF_4$: Yb^{3+}/Ho^{3+} crystals can be also tuned to red by codoping Ce^{3+} ions, but the tunable regions of UC emission are different for different host morphologies. Therefore, the region, respectively, as shown in Fig. 9(d). Thus, the UC emission of β-$NaYF_4$: Yb^{3+}/Ho^{3+} crystals can be also

tuned to red by codoping Ce^{3+} ions, but the tunable regions of UC emission are different for different host morphologies. Therefore, the tunable fluorescence emission not only depends on the sensitized ion, but also relies on the morphology and the host matrix.

4. Conclusions

The UC luminescence emission were successfully tuned in β-$NaY(Gd_{0.4})F_4$: Yb^{3+}/Ho^{3+} nanorods by introducing Ce^{3+} ions. The effects of Ce^{3+} ions on the UC luminescence of the nanorods were studied with 980 nm excitation, and the corresponding mechanism was investigated. It was found that the R/G ratio was increased by increasing Ce^{3+} concentration, which were primarily attributed to the two efficient CR processes of $^5S_2/^5F_4$ (Ho^{3+}) + $^2F_{5/2}$ (Ce^{3+}) $\rightarrow$$^5F_5$ (Ho^{3+}) + $^2F_{7/2}$ (Ce^{3+}) and $^5I_6$ (Ho^{3+}) + $^2F_{5/2}$ (Ce^{3+}) $\rightarrow$$^5I_7$ (Ho^{3+}) + $^2F_{7/2}$ (Ce^{3+}) between the Ho^{3+} and Ce^{3+} ions. The conversion efficiency of CR1 and CR2 was calculated base on steady-state equations, which indicated that the CR2 process plays the assistant role for the CR1 process to covert the green UC emission into red UC emission. Further observation on the color change of UC emission from β-$NaYF_4$: Yb^{3+}/Ho^{3+} microplates and microprisms through codoping Ce^{3+} suggested that Ce^{3+} is an effective sensitizer to tune UC emission for extending their application in display and biological images, and the color tuning range and emission intensity also were affected by host material and morphology of particle samples.

The work is supported by the National Science Foundation of China (Grant 11174190), the Fundamental Research Funds for the Central Universities (Grants GK201101006 and GK201304002).

Notes and references

[a] *School of Physics and Information Technology, Shaanxi Normal University, Xi'an 710062, P.R. China . Fax：86 029 8530 3575 E-mail: hrzheng@snnu.edu.cn*

†Electronic Supplementary Information (ESI) available: [details of any supplementary information available should be included here]. See DOI: 10.1039/b000000x/

‡Footnotes should appear here. These might include comments relevant to but not central to the matter under discussion, limited experimental and spectral data, and crystallographic data.

1 R. Bhargava, D. Gallaghar, X. Hong and A. Nurmikko, *Phys. Rev. Lett*., 1994, **72**, 416.

2 D. Q. Chen, L. Lei, Yang A P, Z. X. Wang and Y. S. Wang, *Chem. Commun.*, 2012,**48**, 5898.

3 B. Vander. Ende, L. Aartsa and A. Meijerink, *Physical. Chemistry. Chemical. Physics*., 2009, **11**, 1108.

4 F. Auzel, *Chemical..Reviews*., 2004, **104**, 139.

5 G. S. Maciel, A. Biswas, R. Kapoor and P. N. Prasad, *Appl. Phys. Lett.*, 2000, **76**, 1978.

6 F. Wang and X. G. Liu ,*Chemical. Society. Reviews*., 2009, **38,** 976.

7 T. S. Yang, Y. Sun, Q. Liu, W. Feng, P. Y. Yang and F. Y. Li, *Biomaterials*., 2012, **33**, 3733.

8 J. F. Suyver, J. Grimm, M. K. Veen, D. Biner, K. W. Kramer and H. U. Gudel, *J.Lumin*., 2006, **117**, 1.

9 N. Menyuk, K. Dwight and J. W. Pierce, *Appl. Phys. Let*.,1972, **21**, 159.

10 J. X. Fu, X. H. Fu, C. M. Wang, X. F. Yang, J. L. Zhuang, G.G.Zhang, B.Y. Lai, M. M. Wu, and J. Wang, *Eur. J. Inorg. Chem.*, 2013, **8**, 1269.

11 S. W. Wu, G. Han, D. J. Milliron, S. Aloni, V. Altoe, D. V. Talapin, B. E. Cohen and P. J. Schuck , *Proc. Natl. Acad. Sci. U. S. A*. 2009, **106,** 10917.

12 G. Y. Yi, D. P. Chen, H. C. Lu, L. H. Guo, S. Y. Zhao, Y. Ge and W. J. Yang, *Nano. Lett*., 2004, **11**, 191.

13 D. L. Gao, H. R. Zheng, X. Y. Zhang, W. Gao, Y. Tian, J. Li and M. Cui, *Nanotechnology*., 2011, **22**, 1.

14 X. C. Ye, J. E. Collins, Y. J. Kang, J. Chen, D. T. N. Chen and A. G. Yodh, *Christopher B. Murray*., 2010, **107**, 22430.

15 Y. Wei, F. Q. Lu, X. R. Zhang and D. P. Chen, *Chem. Mater*., 2006, **18**, 5733.

16 J. L. Zhuang, X. F.Yang, J.X. Fu, C.L. Liang, M. M. Wu, J.Wang and Q.Su, *Cryst. Growth Des.*, 2013，13, 2292.

17 J. L. Zhang, J. Wang, X. F. Yang, I. D. Williams, W. Zhang, Q. Y. Zhang, Z. M. Feng, Z. M. Yang, C. L. Liang, M. M.Wu and Q. Su , *Chem. Mater*., 2009, **21**, 160.

18 C. X. Li, J. Yang, Z. W. Quan, P. P. Yang, D. Y. Kong and J. Lin , *Chem. Mater*., 2007, **19**, 4933.

19 Q. Wang, Y. X. Liu., B. C. Liu, Z. L. Chai, G. R. Xu, S. L. Yu, and J . Zhang, *Cryst. Eng. Comm*., 2013, **15**, 8262.

20 D. L. Gao, X. Y. Zhang, W. Gao, *Appl. Mater. Interfaces.*, 2013, **5**, 9732.

21 F. Wang, Y. Han, C. Lim, Y. Lu, J. Wang, J. Xu, H. Chen, C. Zhang, M. Hong, X. Liu, *Nature Lett.,* 2010, **463**, 1061.

22 D. Q. Chen, Y. L. Yu, F. Huang, A. P. Yang and Y. S. Wang, *J Mater Chem*., 2011, **21**, 6186.

23 L. Lei, D. Q. Chen, P. Huang, J. Xu, R. Zhang and Y. S.Wang, *Nanoscale*., 2013, **5**, 11298.

24 E. M. Chan, G. Han, J. D. Goldberg, D. J. Gargas and A. D. Ostrowski, *Nano Lett.*, 2012, **12**, 3839.

25 D. Q. Chen, Y. L. Yu, F. Huang and Y. S. Wang, *Chem. Commun*., 2011, **47**, 2601.

26 D. L. Gao, X. Y. Zhang and W. Gao, *J. Appl. Phys.*, 2012, **111**, 033505.

27 H. Guo, Z. Q. Li, H. S. Qian, Y. Hu and N. M. Idris, *Nanotechnology.*, 2010, **21**, 125602.

28 W. Song, A. E. Vasdekis, Z. Li and D. Pstaltis, *Appl. Phys.Lett.*, 2009, **94**, 051117.

29 F. Wang and X. G. Liu, *J. Am. Chem. Soc.*, 2008, **130**, 5642.

30 G. Tian, Z. J. Gu, L. J.Zhou, W. Y. Yin, X. X. Liu, L. Yan, S. Jin, W. L. Ren, G. M. Xing, S. Y. Li, and Y. L. Zhao, *Adv. Mater*., 2012, **24**, 1226.

31 L. L. Wang, M. Lan, Z. Y. Liu, G. S. Qin, C. F. Wu, X. Wang, W. P. Qin, W. Huang and L. Huang , *J. Mater. Chem. C.*, 2013, **1**, 2485.

32 X. X. Zhang, P. Hong, M. Bass and B. H. T. Chai, *Appl. Phys. Let.,* 1993, **63**, 2606.

33 T. Li, C. F. Guo, Y. M. Yang, L. Li and N. Zhang, *Acta. Materialia.*, 2013, **61**, 7481.

34 Y. S. Chen, X. L. Hao, J. P. Zhou, Y. C. Jiao, W. He, H. H. Wang, J. X. Lu, S. E. Yang, *Matter. Lette*., 2012, **83**, 49.

35 G. S. Yi and G. M. Chow, *J. Mater. Chem.* 2005, **15**, 4460.

36 R. Lisiecki, G. Dominiak-Dzik, W. Ryba-Romanowski and T. Lukasiewicz, *J. Appl. Phys*., 2004, **96**, 6323.
37 G. Y. Chen, H. C. Liu, G. Somesfalean, H. J. Liang and Z. G. Zhang, *Nanotechnology.*, 2009, **20**, 385704.
38 L. L. Tao, Y. H. Tsang, B. Zhou, B. Richards and A. Jha, *Journal of Non-Crystalline Solids*., 2012, **358**, 1644.
39. K. W. Krämer, D. Biner, G. Frei, H. U. Güdel, M. P. Hehlen and S. R. Lüthi, *Chem. Mater.,* 2004, **16**, 1244.
40 S. Heer, K. Kömpe, H. U. Güdel and M. Haase, *Adv. Mater*., 2004, **16**, 2102.
41 X. C. Ye, J. E. Collions, Y. J. Kang, J. Chen, D. T. N. Chen, A. G. Yodh and C. B. Murray, *PNAS*., 2010, **107**, 22430-5.
42 R. D. Shannon, *Acta Crys tallogr. A.,* 1976, **32**, 751.
43 Q. Q. Dou and Y. Zhang, *Langmuir.*, 2011, **27**, 13236.
44 H. X. Mai, Y. W. Zhang, R. Si, Z. G. Yan, L. D. Sun, L. P. You and C. H. Yan , *J. Am. Chem. Soc*., 2006, **128**, 6426.
45 G. Blasse and B. C. Grabmaier, *Luminescent materials.*, Berlin, Springer-Verlag, 1994.
46 J. H. Chung, S. Y. Lee, K. B. Shim and J. H. Ryu, *Appl. Phys. Exp*., 2012, **5**, 052602.
47 R. P. Leavitt, J. B. Gruber, N. C. Chang and C. A. Morrison, *J. Chem. Phys*., 1982, **76**, 4775.
48 De. La. E. Rosa, P. Salas, H. Desirena, C. Angeles and R. A. Rodríguez, *Appl. Phys. Lett*., 2005, **87**, 241912.
49 L.Y.Wang and Y.D. Li, *Nano Lett*., 2006, **8**, 1645.